Journal of Marine Systems 148 (2015) 236–248

Contents lists available at ScienceDirect

Journal of Marine Systems

journal homepage: www.elsevier.com/locate/jmarsys

Effect of steady and unsteady flow on chemoattractant plume formation and sperm taxis

Allison F. Bell, John P. Crimaldi *

Department of Civil, Environmental and Architectural Engineering, University of Colorado, Boulder, CO 80309-0428, USA

ARTICLE INFO

Article history:
Received 30 September 2014
Received in revised form 27 February 2015
Accepted 16 March 2015
Available online 27 March 2015

Keywords:
Chemotaxis
Gametes
Broadcast spawning

ABSTRACT

The formation of chemoattractant plumes around benthic invertebrate eggs in steady and unsteady shear flows is investigated for a range of shear rates, and the ability of sperm to navigate within these plumes is assessed using several chemotactic strategies. Although many of the details of sperm taxis remain uncertain, we investigate the role of basic processes using a toy model in two dimensions. Search strategies in 2D are intrinsically less complex than 3D, but many of the basic components are similar, and the simplified geometry permits an understanding and identification of the key factors of navigation tactics. Numerical simulations are used to model the advection and diffusion of the chemoattractant within the different flows, using three different sperm swimming behaviors. A Monte-Carlo approach is then used to determine the probability of a sperm reaching an egg for a range of flow conditions, initial conditions, and swimming behaviors. The spatial structure of chemoattractant plumes at the scale of the gametes is also investigated. Success rates for locating an egg decrease monotonically with increasing shear rates, and a definitive hierarchical ordering of the tested swimming strategies is identified. A conceptual framework to study and identify important aspects of this fundamental process to support further studies is provided.

1. Introduction

A variety of benthic invertebrates use broadcast spawning as a reproductive strategy. Sessile adult males and females, separated by a distance on the order of meters, synchronously release sperm and eggs into the ambient flow. Although sperm are motile, their swimming speed is likely too slow to bridge the initial distance to the closest eggs, so physical stirring by the large-scale flow is required to aggregate the gametes. Meanwhile, eggs increase their effective target size by emitting plumes of chemoattractant that are stirred and stretched by the local small-scale flow. If flow processes advect sperm sufficiently close to eggs, motile sperm employ chemotaxis to navigate through gradients in the chemoattractant plumes to help locate and fertilize the egg.

From release to fertilization, spawned gametes traverse a physiochemical environment with features that span spatial scales from microns to meters. The impact of these physical and chemical processes at various scales on the resulting efficacy of the fertilization strategy is difficult to study and not well understood. Various large-scale flow phenomena have been proposed to produce gamete aggregation, but the evidence for this is still indirect. At the small-scale end of the spectrum, details of the nature of chemoattractant plumes in realistic flow conditions are all but unknown, as are details of how sperm navigate within complex chemical landscapes. For a review of the current state of knowledge on the impact of flow on fertilization success across a range of scales, see Crimaldi and Zimmer (2014). In the present study, we focus on the small-scale aspects of the problem. We use analytical and numerical models of fluid flow, chemoattractant plume dispersion, and sperm motility and chemotaxis to investigate how unsteady and spatially varying flow processes shape chemoattractant plumes and impact fertilization success at the gamete scale. The study is necessarily idealized by design, given that many of the specific details about various constitutive aspects of the problem are not easily observed or documented using current experimental and laboratory techniques.

1.1. Background

Sperm exhibit a chemotactic response to chemicals released by conspecific eggs for a range of benthic invertebrates including urchin (Böhmer et al., 2005; Kaupp et al., 2003), star fish (Böhmer et al., 2005), sea squirt (Jantzen et al., 2001), siphonophores (Cosson et al., 1984), coral (Morita et al., 2006) and abalone (Riffell et al., 2002). Sperm response behavior is observed when the chemoattractant concentration is above a given threshold (Riffell et al., 2004; Zimmer and Riffell, 2011), and in the presence of a chemoattractant gradient (Riffell et al., 2002, 2004; Ward et al., 1985).

We base the present study on known chemoattractant characteristics associated with gametes of red abalone (*Haliotis rufescens*) because gametes of this organism have been extensively studied. For red abalone, the chemoattractant released by eggs has been identified as the free

* Corresponding author at: 428 UCB University of Colorado Boulder, CO 80309-0428.
E-mail address: crimaldi@colorado.edu (J.P. Crimaldi).

http://dx.doi.org/10.1016/j.jmarsys.2015.03.008
0924-7963/

amino acid L-tryptophan (Riffell et al., 2002), which is released at a relatively constant flux in the range of 0.18–0.3 mol egg^{-1} min^{-1} (Himes et al., 2011; Krug et al., 2009) for 45 min after being spawned (Himes et al., 2011; Krug et al., 2009). Typical of amino acids, L-tryptophan is weakly diffusive in water, with a reported diffusivity of 6×10^{-9} m^2 s^{-1} (Mark and Nilsson, 2002; Polson, 1937; Zimmer and Riffell, 2011). The threshold concentration of L-tryptophan that elicits chemotactic response in red abalone sperm is reported to be between 3×10^{-10} mol L^{-1} and 4×10^{-9} mol L^{-1} (Riffell et al., 2004; Zimmer and Riffell, 2011).

Much less is known about the behavioral response characteristics of sperm to an associated chemoattractant. Therefore, in this work, we synthesize sperm behavioral response information from a range of benthic invertebrate species. Sperm of most species have similar swimming patterns, resulting from the helical motion of a flagellum (Friedrich and Julicher, 2009), although the resulting swimming speeds are highly variable even within one species (Kupriyanova and Havenhand, 2002).

The paths of swimming sperm have been observed in the field (Babcock et al., 1994; Miller and Mundy, 2005; Quinn and Ackerman, 2011), and more typically under a microscope (Böhmer et al., 2005; Cosson et al., 1984; Evans et al., 2012; Guerrero et al., 2010a; Himes et al., 2011; Inamdar et al., 2007; Morita et al., 2006; Riffell and Zimmer, 2007; Riffell et al., 2002, 2004; Wood et al., 2005; Yoshida et al., 1993; Zimmer and Riffell, 2011) leading to a basic understanding of swimming patterns and parameters. Two distinct sperm behaviors have been observed: one (called loitering behavior) corresponding to sperm exposed to a chemoattractant concentration below the response threshold, and the other (called response behavior) corresponding to exposure above the threshold. Most documented loitering behaviors consist of chiral beats resulting in helical paths (in 3D) (Friedrich and Julicher, 2007, 2009; Riffell and Zimmer, 2007) or drifting circles (in 2D) (Alvarez et al., 2012; Böhmer et al., 2005; Friedrich and Julicher, 2008; Kaupp et al., 2008). Sperm swimming near a surface or boundary exhibit characteristics of 2D swimming and no longer swim in helical paths, but instead move in drifting circles (Alvarez et al., 2014). Within the loitering behavior, no bias with respect to an egg has been observed (Morita et al., 2006; Riffell and Zimmer, 2007; Riffell et al., 2002, 2004; Vogel et al., 1982). The path is considered random outside any stimulus.

There is greater variation in the documented response behaviors. It is known that receptors on the flagellum register a change in the chemoattractant concentration and initiate a chain of chemical reactions within the sperm that control its behavior (Alvarez et al., 2012; Böhmer et al., 2005; Guerrero et al., 2010a,b; Kaupp et al., 2003; Morita et al., 2009; Wood et al., 2005; Yoshida and Yoshida, 2011). It is not fully understood if sperm can determine the gradient due to a Lagrangian or spatial change registered along the flagellum. As the sperm swims and monitors the gradient, it is able to perceive the spatial concentration gradient and the flagellum reacts physically to move the sperm up-gradient (Alvarez et al., 2014). The observed changes due to stimuli are varied, but two major components are consistent. The response is manifested in a change in direction (chemotaxis) and/or a change in swimming speed (chemokinesis). It is not clear if chemokinesis always accompanies chemotaxis and as Kupriyanova and Havenhand (2002) noted, current studies do not clearly distinguish chemokinesis from chemotaxis. The theoretical description of chemotaxis and the effective diffusivity of searching sperm modeled in Friedrich and Julicher (2008) consider only a directional response with a constant speed unchanged by stimuli. The addition of chemokinesis can alter the swimming path in a few ways: a decrease in the curvature resulting in an increased drifting speed (Riffell et al., 2004; Ward et al., 1985; Zimmer and Riffell, 2011), a path described as a trochoid or prolate trochoid (Böhmer et al., 2005; Guerrero et al., 2010b; Kaupp et al., 2006, 2008), severe suppression of turns such that any turns are no longer recognized (Guerrero et al., 2010a; Riffell et al., 2004), or a doubling of the swimming speed performed in straight run (Riffell and Zimmer, 2007; Riffell et al., 2004; Zimmer and Riffell, 2011).

Mathematical modeling of the mechanics of broadcast spawning has contributed to a better understanding of the mechanics. To replicate sperm motility, previous studies have modeled the swimming paths as a diffusive process (Alt, 1980; Babcock et al., 1994; Keller and Segel, 1971). When chemotaxis is considered, sperm paths have been modeled as a biased random-walk (Alt, 1980; Jabbarzadeh and Abrams, 2005) and as a diffusive process wherein the diffusivity of the linear path is relative to the strength of the chemoattractant (Friedrich and Julicher, 2008, 2009). Yoshida et al. (1993) developed the widely used linear equation chemotaxis index (Guerrero et al., 2010a; Yoshida et al., 2002), which measures the trajectory of the sperm relative to the egg, in order to quantify chemotaxis. Sperm velocity and orientation relative to the egg have been calculated to indicate the linearity of the path and the increase in swimming speed as well (Himes et al., 2011; Riffell et al., 2004; Zimmer and Riffell, 2011). Models have also been used to estimate fertilization rates using a variety of techniques: an advection–diffusion process (Kiselev and Ryzhik, 2012), probability of collision (Vogel et al., 1982), and a function of egg diameter and sperm concentration (Vogel et al., 1982).

Other search strategies, such as intermittent search behaviors, persistent random walks and infotaxis have been analyzed to determine their effectiveness. Intermittent search behaviors have been observed in a variety of cases, such as animals looking for shelter and proteins seeking a site on a DNA molecule (Benichou et al., 2011). Benichou et al. (2007) determined analytically that this process can be optimized and found that search times associated with no temporal or orientational memory, such as sperm navigating a chemoattractant plume, are within an order of magnitude of search times that are associated with a memory. Persistent random walks have been used to determine the probability of sperm locating an egg, in addition to creating a scaling law for optimization of the search by using the persistence length, target distance and search time (Friedrich, 2008). Vergassola et al. (2007) used a computational model to introduce 'infotaxis' as a method of locating a target when there is minimal or inconsistent information. An example of this could be a sperm searching for an egg in a turbulent flow that serves to disconnect and dilute the chemoattractant plume. In the 'infotaxis' strategy, the searcher determines the optimum direction to maximize the rate of useful information at each time-step and it is suggested that this could be attributed to a broader range of search strategies where there is minimal information.

In addition to the biological aspects of the problem, flow dynamics at the gamete scale have been identified and used to study fertilization mechanics. The typical environment where benthic invertebrates spawn is turbulent, but with relatively low mean velocities (Zimmer and Riffell, 2011). The magnitude of the Kolmogorov scale in these environments is on the order of millimeters. Sperm and egg dimensions are on the order of micrometers, smaller than the Kolmogorov scale. Therefore, gametes experience a physical world dominated by a single dissipative vortex at any given time. This results locally in a linear shear (Jumars et al., 2009; Karp-Boss et al., 1996; Riffell and Zimmer, 2007; Zimmer and Riffell, 2011).

Zimmer and Riffell (2011) modeled the development of chemoattractant plumes in steady shear using a numerical simulation, and tested the impact of shear rates on fertilization rates experimentally for red abalone using a Taylor–Couette flow. Fertilization was enhanced for shear rates less than $\alpha = 1$ s^{-1}, yet fertilization decreased in shear rates exceeding $\alpha = 1$ s^{-1} (Riffell and Zimmer, 2007; Zimmer and Riffell, 2011). Increases in energy dissipation rates (Denny et al., 2002), bed roughness (Quinn and Ackerman, 2011), flow velocity (Levitan et al., 1992) and turbulence (Denny and Shibata, 1989; Denny et al., 1992; Levitan and Young, 1995) have also been shown to decrease success rates. Additionally, the preference of a sperm for certain eggs within a single species (Evans et al., 2012), and viability of both the egg and sperm (Giorgi and DeMartini, 1977) can decrease actual and predicted fertilization rates. In the absence of flow, the effective target size of the egg increases fertilization rates and decreases the

negative impact of sperm limitation and sperm dilution (Farley, 2002; Farley and Levitan, 2001; Jantzen et al., 2001; Levitan, 1993, 1996, 2000, 2006; Levitan and Irvine, 2001; Styan, 1998).

1.2. Present study

In the current study we use a series of numerical simulations to model interactions of small-scale physical–biological processes in broadcast spawning. We model a flow field consisting of shear that is unsteady in both direction and magnitude. This flow field is representative of flow experienced by gamete-scale (sub-Kolmogorov) particles within larger-scale turbulence. The flow is modified by the presence of a freely rotating and advecting egg. We then use the model to determine the unsteady spatial distribution of chemoattractant released by the egg. The chemoattractant distribution is governed by stirring from the local flow and by molecular diffusion. Finally, we use the model to determine sperm trajectories for several behavioral strategies as the sperm navigate through the chemoattractant plume. Ultimately, we gain insight into the role of turbulent flow on shaping gamete-scale chemoattractant plumes, and on the role of several behavioral strategies used by sperm to enhance their likelihood of locating an egg.

Searching for a target in 2D is intrinsically easier than in 3D, but many of the fundamental challenges remain. In the present study, the problem is studied using a toy model in the simpler 2D space; the goal of the resulting simulations is to investigate the process-level role of structured stirring on the attractant plume formation and chemotaxis efficacy, and to build a framework for understanding more complex flows. It is common to investigate the mechanistic features of complex 3D stirring processes with simpler 2D models (e.g., Basu et al., 2007; Cetegen and Mohamad, 1993; Crimaldi et al., 2006, 2008; Flohr and Vassilicos, 1997; Martinand and Vassilicos, 2007; Meunier and Villermaux, 2003; Rehm et al., 1993); these models elucidate instantaneous processes seen locally in more complex 3D flows. Ultimately, the present model can serve as a stepping stone for more complex models in the future.

2. Methods

2.1. Numerical modeling of plume development at the scale of an egg

2.1.1. Steady shear flow

The distribution of chemoattractant mass is modeled for steady and unsteady linear shear flows. A linear shear flow in the x-direction with shear rate α is given by $\vec{u} = (\alpha y, 0)$. In the presence of a freely rotating round egg, the shear flow is modified locally such that the x and y velocity components are given by (Mikulencak and Morris, 2004)

$$\frac{u_x}{\alpha R_{egg}} = \frac{1}{2}y^*\left(1-r^{*-4}\right) + \frac{1}{2}y^*\left(1-r^{*-2}\right) - 2x^{*2}y^*\left(r^{*-4}-r^{*-6}\right) - \frac{-\frac{1}{2}y^*}{r^{*2}} \quad (1)$$

$$\frac{u_y}{\alpha R_{egg}} = \frac{1}{2}x^*\left(1-r^{*-4}\right) + \frac{1}{2}x^*\left(1-r^{*-2}\right) - 2x^*y^{*2}\left(r^{*-4}-r^{*-6}\right) - \frac{-\frac{1}{2}x^*}{r^{*2}} \quad (2)$$

where $x^* = \frac{x}{R_{egg}}, y^* = \frac{y}{R_{egg}}, r^* = \frac{r}{R_{egg}}$, r is radial distance from the center of the egg and $R_{egg} = 100\,\mu m$ and is the radius of the egg. The streamlines associated with this flow are shown in Fig. 1 for $\alpha = 1\ s^{-1}$.

Constant shear rates $\alpha = 0, 0.1, 0.2, 0.4, 1, 2\ s^{-1}$ are used in the model, where $\alpha = 0$ corresponds to a quiescent case. Zimmer and Riffell (2011) show that for shear rates exceeding $2\ s^{-1}$, the ability of the sperm to turn decreases and this reduces their ability to find an egg, so we limit the shear rate below the level where it begins to impact sperm motility. Shear causes eggs to rotate at a rate proportional to the shear strength. At shear rates exceeding $1\ s^{-1}$, the rotation significantly decreases the ability of a sperm to successfully attach to an egg after it is found (Riffell and Zimmer, 2007). This effect is not incorporated into this study and is only one of several factors that can impede fertilization once the sperm locates an egg. The relative importance of shear rate on plume formation depends on the value of chemoattractant diffusivity D. Using α^{-1} and R_{egg}^2/D as characteristic timescales for advection and diffusion, respectively, we can define a Péclet number as $Pe = \frac{\alpha R_{egg}^2}{D}$ (see Table A.1 for values). The Péclet values associated with the steady shear flows in the model are 1.5, 3, 6, 15 and 30.

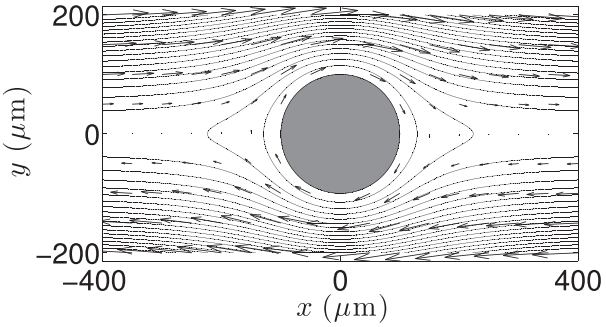

Fig. 1. Streamlines (black lines) and velocity vectors (black arrows) for the steady shear flow with shear rate $\alpha = 1\ s^{-1}$ in the presence of an egg (gray circle). The streamlines indicate that the flow near the surface of the egg is circular and that velocity increases away from the egg.

2.1.2. Unsteady shear flow

We also consider a more complex flow that mimics an egg in an unsteady, turbulent flow. At any instant, the egg is assumed to be in the middle of a single Kolmogorov-scale vortical flow structure, with locally linear shear. We use Eqs. (1) and (2) to define the linear shear flow, but the direction and magnitude of the shear now changes with time.

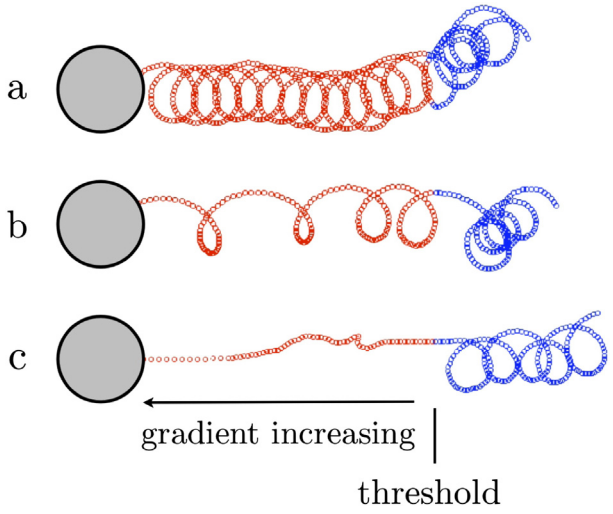

Fig. 2. A depiction of each response behavior taken from actual model simulations: (a) Drifting Circle, (b) Turn and Run, and (c) Run. The egg is indicated by the gray circle, the loitering path is shown with the blue circles and the red circles show the response behavior. Each circle represents a time-step. The gradient magnitude is increasing from right to left and the threshold boundary is indicated by the vertical line. (For interpretation of the references to color in this figure legend, the reader is referred to the web version of this article.)

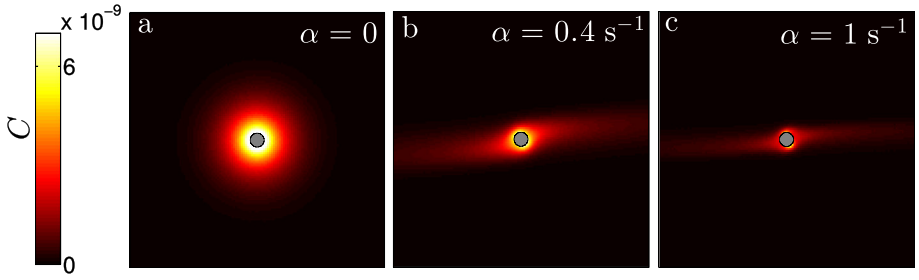

Fig. 3. Steady-state chemoattractant distributions for steady shear flows at three different values of α. The 200 μm egg is indicated by the gray circle.

The direction of the shear, defined as angle ϕ from the horizontal, is updated at each time-step dt by sampling from a normal distribution according to

$$\phi_{new} = \phi_{old} + \dot{\phi}\ \ dt, \tag{3}$$

where $\dot{\phi}$ is a normally distributed random variable red with units of s^{-1}, zero mean and standard deviation $\sigma_{\dot{\phi}}$ (Table A.1). The magnitude of the shear is varied as

$$\alpha(t) = \alpha_0\ \ \sin(t/T), \tag{4}$$

where the amplitude α_0 has is different for two cases: low ($\alpha_0 = 0.5\ s^{-1}$) and high ($\alpha_0 = 1.25\ s^{-1}$).

The radius of the vortex is held constant for simplicity. The decay rate used to replicate the decay in velocity from the center of the vortex corresponds to the shear stress decay associated with an Oseen vortex (Panton, 1996) written as

$$h(r) = \frac{1}{(r/r_{core})^2}\left[1 - \exp\left[-\left(\frac{r}{r_{core}}\right)^2\right]\right] \tag{5}$$

where r_{core} is the scale for the rotational core of the eddy (Table A.1) and is below the Kolmogorov scale.

2.1.3. Chemoattractant flux model

We use a quasi-2D model with a domain consisting of a thin sheet passing through the center of an egg. The chemoattractant release into the domain thus comes from a circumferential band consisting of the intersection of the surface of the egg with the sheet. We use a flux rate of 2.38×10^{-23} mol $\mu m^{-2}\ s^{-1}$ calculated from the total release rate of 0.18 fmol egg^{-1} for a 200 μm red abalone egg given by Zimmer and Riffell (2011). The mass of chemoattractant is released 25 μm inside the surface of the egg to account for the existence of a jelly coat. We assume the same diffusivity within the jelly coat.

We model the release, transport and dispersion of the chemoattractant tryptophan using a Lagrangian particle tracking method (Kinzelbach, 1988) with 1×10^6 particles per simulation. These particles then diffuse outward via a random-walk method and advect passively in the flow (Eqs. (1) and (2) for the steady shear flows and Eqs. (1)–(5) for the unsteady shear cases). The 2D particle positions x_n at time-step n in flow $\vec{u}$ are computed via

$$\vec{x}_n = \vec{x}_{n-1} + \vec{u}\left(\vec{x}_{n-1}\right)dt + \vec{Z}\sqrt{2Ddt}, \tag{6}$$

where D is the molecular diffusivity of tryptophan (Table A.1) and $\vec{Z}$ is a random vector where each component has a normally distributed magnitude with a mean of zero and variance of one. Each particle has a constant molar mass. Particles are binned over small regions and concentrations are calculated by counting the number of particles per area and multiplying by the molar mass per particle. The model is run

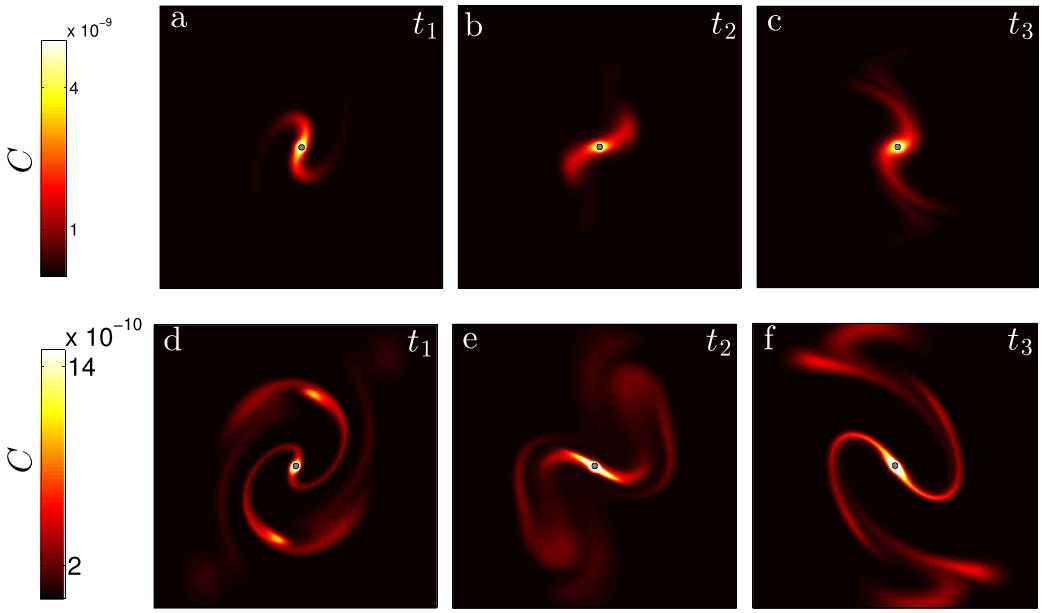

Fig. 4. Three representative slices at 60-second intervals of the chemoattractant distributions for unsteady shear flows where $\alpha_0 = 0.5\ s^{-1}$ (a–c) and $\alpha_0 = 1.25\ s^{-1}$ (d–f). The plumes were allowed to develop over an initial 3-minute period. The 200 μm egg is indicated by the gray circle.

until the concentration fields reach a local steady-state for the steady shear flows, and until the plumes are fully developed in the unsteady shear flow (typically about 3 min). The stochastic structure of the chemoattractant plume remains approximately constant after this 3 minute period, and at times before this, the plume is similar to those in the steady shear flow cases.

2.2. Model for loitering behavior

Motile sperm are also modeled via a Lagrangian approach. In order to gather statistics about sperm paths and fertilization rates, we use 5×10^5 sperm in each simulation. The sperm are advected passively by the flow, but also move actively according to a prescribed swimming behavior. The sperm exhibit a loitering behavior if the local concentration is below a threshold or in the absence of a gradient regardless of the local concentration.

The most commonly observed loitering behavior is accomplished in the model by the superposition of a circular velocity and a drifting velocity. The exact mechanics of this process are still not fully understood. Numerous studies have identified constituent motions including circling (Alvarez et al., 2012; Böhmer et al., 2005; Friedrich, 2008; Kaupp et al., 2003; Wood et al., 2005), drifting (Böhmer et al., 2005; Friedrich, 2008; Kaupp et al., 2003) and running (Guerrero et al., 2010b; Riffell et al., 2004). This model is a composite of those behaviors in which we can vary different aspects to examine relative contributions of each motion. It is meant to be representative of the statistical motion of a collection of sperm. In all cases, the velocity of the swimming sperm is

$$\vec{v} = \vec{v}_{\text{circ}} + \vec{v}_{\text{drift}} + \vec{v}_{\text{run}}, \tag{7}$$

where $\vec{v}_{\text{circ}}$ consists of swimming speed v_c and turning rate $\dot{\theta}$, $\vec{v}_{\text{drift}}$ consists of drifting speed v_d and drifting direction θ_d, and $\vec{v}_{\text{run}}$ consists of swimming speed v_r and direction θ_r. The sperm positions at time-step n are determined by the swimming velocity $\vec{v}$ and the flow $\vec{u}$ as

$$\vec{x}_{s_n} = \vec{x}_{s_{n-1}} + \vec{u}\left(\vec{x}_{n-1}\right)dt + \vec{v}\left(\vec{x}_{s_{n-1}}\right)dt. \tag{8}$$

The loitering velocity in the model is given by Eq. (7), where v_c is held constant and the turning rate $\dot{\theta}$ varies over time such that it is normally distributed with mean $\mu_{\dot{\theta}}$ and standard deviation $\sigma_{\dot{\theta}}$ (Table A.1). This initial swimming direction for each sperm is chosen randomly from $[0, 2\pi]$. The speed v_d varies over time such that it has a triangle distribution centered on v_d, tapering linearly to zero at $v_d \pm \Delta v_d$ value found in Table A.1. Note that the triangle distribution is used to avoid the possibility of nonphysical behavior associated with the infinite tail of a normal distribution. The direction θ_d, is initially chosen randomly from $[0, 2\pi]$ and varies over time such that it has a triangle distribution centered on θ_d, tapering linearly to zero at $\theta_d \pm \Delta\theta_d$ (Table A.1). For loitering, $\vec{v}_{\text{run}} = 0$. The swimming parameters were chosen to agree with the observations of Böhmer et al. (2005), Kaupp et al. (2003), Wood et al. (2005) and extant models (Friedrich and Julicher, 2008) and to relate to observations of swimming sperm.

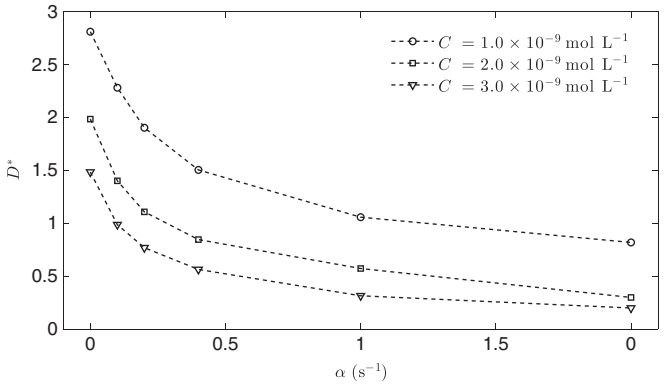

Fig. 6. The effective diameter D^* as a function of steady shear rate α for three threshold concentration values.

2.3. Model for response behavior

Three distinct behaviors are established to model the range of observed chemotactic and chemokinetic strategies employed by sperm responding to a stimulus: I) Drifting Circle, II) Turn and Run, and III) Run. Sperm with no response to stimuli are also modeled as a base case. Sperm exhibit a response behavior for all time when the local concentration exceeds a threshold concentration and maintain or revert to a loitering behavior when the local concentration is less than the threshold level or the gradient is zero. A concentration gradient vector is calculated at the location of the sperm using the local structure of the chemoattractant plume at that time. It is assumed that the sperm have access to this information and are continually monitoring the space around them, as indicated by previous studies (Alvarez et al., 2014).

I) The Drifting Circle Response models sperm that use chemotaxis, but not chemokinesis (change speed due to stimulation). This behavioral response examines the success of sperm that use only chemotaxis and do not change speed when stimulated such as those observed by Kupriyanova and Havenhand (2002). This behavior is modeled as the superposition of a circular motion ($\vec{v}_{\text{circ}}$) with constant curvature (turning rate $\dot{\theta}$ and speed v_c) and a translational drift motion ($\vec{v}_{\text{drift}}$) of constant speed (v_d), but time-dependent direction (θ_d) that depends on the local gradient. θ_d varies over time such that it has a triangle distribution centered on θ_{Ψ^*}, the direction of the local gradient, tapering linearly to zero at $\theta_{\Psi^*} \pm \Delta\theta_d[1-\Psi^*]$. The value for $\Delta\theta_d$ is found in Table A.1. Ψ^* is the non-dimensional magnitude of the local concentration gradient, Ψ, normalized by Ψ_0, the

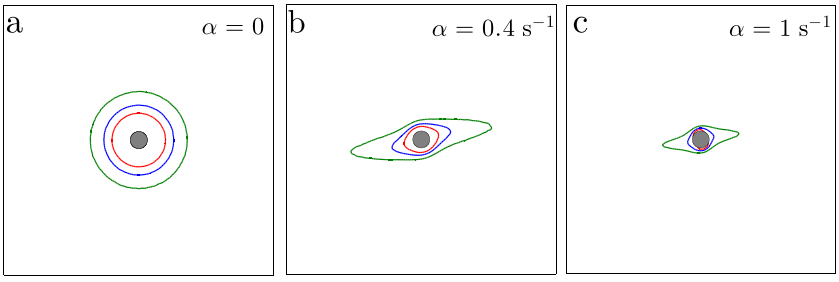

Fig. 5. Steady shear flow contour levels for three threshold concentrations (1×10^{-9} mol L^{-1} (green); 2×10^{-9} mol L^{-1} (blue); 3×10^{-9} mol L^{-1} (red)) for 3 shear rates. These images correspond directly to the concentration images shown in Fig. 3. The gradients are everywhere normal to the contours. The green line depicts the threshold concentration used in the fertilization models. This lies on the higher end of the documented threshold concentration ranges (3×10^{-10} mol L^{-1}–4×10^{-9} mol L^{-1}) (Riffell et al., 2004; Zimmer and Riffell, 2011). The 200 μm egg is indicated by the gray circle. (For interpretation of the references to color in this figure legend, the reader is referred to the web version of this article.)

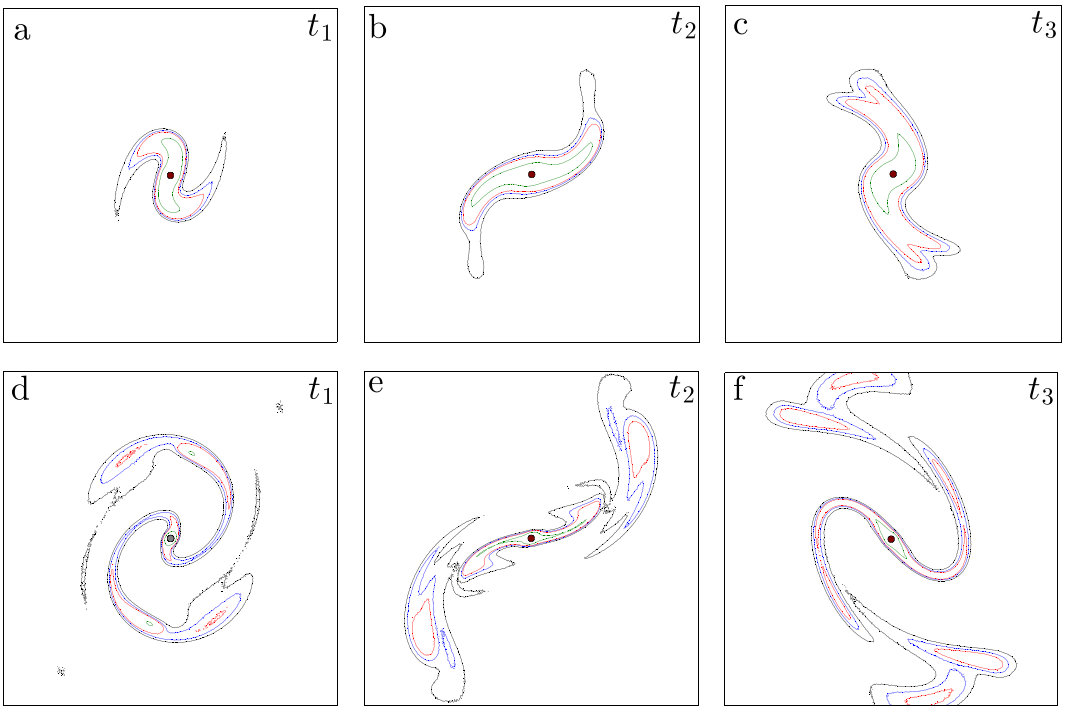

Fig. 7. (a–c) Unsteady shear flow contour levels for the low-α_0 for one minute time intervals. (d–f) High-α_0 cases for the same intervals. Four possible threshold values (1×10^{-10} mol L^{-1} (black); 2×10^{-10} mol L^{-1} (blue); 3×10^{-10} mol L^{-1} (red); 1×10^{-9} mol L^{-1} (black)) are depicted. These images correspond directly to the concentration images shown in Fig. 4. Note that the smallest contour (green) represents a concentration of 1×10^{-9} mol L^{-1}, the threshold concentration used for the steady shear flows, but that the value used for the complex cases is on the lower end of the range at 1×10^{-10} mol L^{-1} (black). The 200 μm egg is indicated by the gray circle. Note that the scale is different from Fig. 5. (For interpretation of the references to color in this figure legend, the reader is referred to the web version of this article.)

maximum chemoattractant gradient in our model domains ($\Psi_0 = 2 \times 10^{-12}$ M μm^{-1}). Ψ^* varies between 0 and 1. When it is closer to 1, the local gradient magnitude is strong so there is minimal variation on the path. When $\Psi^* = 1$, the sperm aligns exactly with the local gradient. When Ψ^* is closer to 0, the local gradient magnitude is weak and there is more variation on the path. For the Drifting Circle Response $\vec{v}_{\text{run}} = 0$. Fig. 2a shows a depiction of this response behavior in a gradient.

II) The Turn and Run Response models sperm with the ability to increase swimming speed and effectively decrease the curvature of the swimming path, consistent with observations made by Böhmer et al. (2005), Guerrero et al. (2010b), Kaupp et al. (2006, 2008), Riffell et al. (2004), Ward et al. (1985), and Zimmer and Riffell (2011). As in the Drifting Circle Response, the path curvature is time-dependent and results from the superposition of a circular motion with a translational motion. In this case, the circular motion ($\vec{v}_{\text{circ}}$) has constant magnitude (v_c) and now also has variable curvature (turning rate $\dot{\theta}$) modulated by the local gradient magnitude. $\dot{\theta}$ changes over time with the local normalized gradient magnitude Ψ^* such that it varies linearly. At each time, the turning rate is determined as

$$\dot{\theta} = \dot{\mu}_\theta \left[1 - a\Psi^*\right], \tag{9}$$

where a is chosen to be 0.5 for our simulations, and $\dot{\mu}_\theta$ is the same mean turning rate used for the loitering behavior (see Section 2.2 and Table A.1). The $\vec{v}_{\text{drift}}$ direction θ_{d} is determined as in the Drifting Circle Response model and the magnitude component v_{d} also varies linearly with Ψ^* and is calculated at each time as

$$v_{\text{d}} = b v_{\text{d}} \left[1 + c\Psi^*\right], \tag{10}$$

where c is chosen to be 1.5 and b is chosen to be 2 so that the velocity at least doubles when the local concentration is above

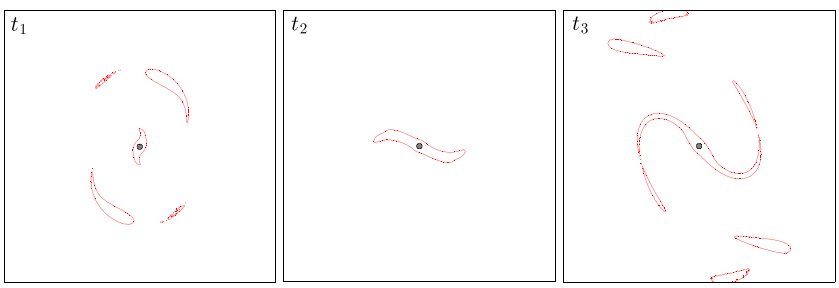

Fig. 8. High-α_0 unsteady shear flow contour levels for concentrations that exceed 3×10^{-10} mol L^{-1} at times corresponding with those in Fig. 7c–e. D_c^* uses the same calculation as Eq. (12), but only the area of contiguous concentration connected to the egg is used for the value of the area.

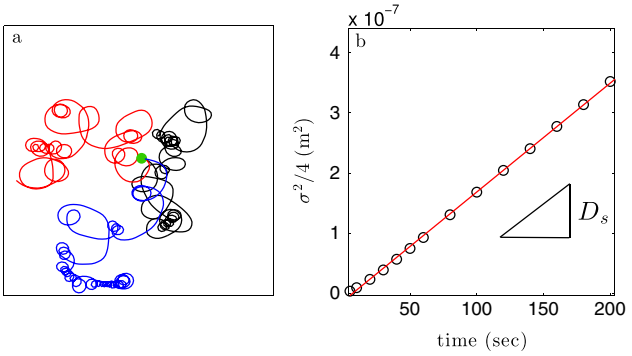

Fig. 9. (a) Three sperm paths (indicated by each color) originating from the same point (indicated by the green dot at the center) at the same time. (b) A plot of $\sigma^2/4$, where σ was calculated from a mass of loitering sperm over the first 200 s, plotted against time (points the open indicated by circles) along with a linear regression line to the points (solid line) used to calculate the diffusivity. The loitering parameters used to calculate the points match the values used in the simulations (Table A.1). (For interpretation of the references to color in this figure legend, the reader is referred to the web version of this article.)

the threshold. $\vec{v}_{run} = 0$ in this case. Unlike previous studies that calculated the variation along the path in a gradient and predicted a diffusion coefficient for a mass of swimming sperm (Friedrich and Julicher, 2008, 2009), here we are implementing these variations and determining their effectiveness on navigation success in a variety of flows. Fig. 2b shows a depiction of this response behavior in a gradient.

III) The Run Response models sperm that abandon the circling strategy of the loitering behavior and execute a run directly upgradient when the local concentration is above the threshold concentration and there is a nonzero gradient. This behavior was chosen due to observations made by Riffell et al. (2004), Riffell and Zimmer (2007), and Zimmer and Riffell (2011) and studies the significance of the circling aspect of the swimming paths. The linear swimming velocity $\vec{v}_{run}$ has magnitude v_r which varies linearly with the local gradient magnitude and is determined at each time via

$$v_r = v_c\left[1 + \Psi^*\right]. \tag{11}$$

The swimming direction θ_r depends on the local gradient and is calculated as θ_d in the Drifting Circle Response. θ_r is calculated at each time from a triangle distribution centered on θ_{Ψ^*}, the direction of the local gradient, tapering linearly to zero at $\theta_{\Psi^*} \pm \Delta\theta_r[1-\Psi^*]$. The value for $\Delta\theta_r$ is in Table A.1. In the Run Response $v_c = v_d = 0$. Fig. 2c shows a depiction of this response behavior in a gradient.

2.4. Fertilization rate model

We use a Monte Carlo approach to calculate the possibility of a sperm reaching an egg. A collection of sperm are placed at one location in the proximity of one egg and simultaneously begin to swim. We assume second-order reaction kinetics based on previous models (Crimaldi et al., 2006; Levitan et al., 1991; Vogel et al., 1982). We present the results as cumulative success rates over time. For simplicity, we consider fertilization as contact with the surface of the egg. While this would not guarantee a successful fertilization, the objective is to understand what impacts the ability of sperm to reach an egg. Additionally, we have not included any modulatory effect of shear in the swimming capability of the sperm by limiting the shear rates (Zimmer and Riffell, 2011).

3. Results

3.1. How flow shapes a 2D chemoattractant plume

Steady-state chemoattractant plume distributions for the steady shear flow at three different values of shear rate α are shown in Fig. 3. The plumes approach a steady-state distribution approximately 3 min after the egg is placed in the flow (the transient response is not shown). The $\alpha = 0$ case (Fig. 3a) corresponds to pure diffusion of chemoattractant in quiescent flow, with a resulting symmetric plume that decays radially away from the egg. As shear rate is increased (Fig. 3b and c), the plume is stretched by the flow into an increasingly elongated filament. This stretching sharpens chemoattractant gradients, increases diffusive flux away from the plume, and decreases local plume concentrations relative to the unsheared case. The shear mechanism responsible for dispersing the chemoattractant is essentially the same as the classic phenomenon described by Taylor (1953), modified locally by the presence of the solid and freely rotating egg. The results shown in Fig. 3 are consistent with steady-shear chemoattractant plumes computed with a similar approach by Zimmer and Riffell (2011).

When shear is unsteady, as it is in turbulent flow, the resulting chemoattractant plumes are more complex (Fig. 4). Using the unsteady shear flow model given by Eqs. (1)–(5), we computed unsteady plume distributions for two values of the unsteady shear amplitude α_0. The plume is allowed to disperse for a period of 3 min after the egg is placed in the unsteady flow such that it reaches a fully developed state across the model domain. The plume, however, continues to change over time in response to the unsteady flow field. To give a sense of the temporal variation in the chemoattractant plume structure, we display in Fig. 3 representative snapshots of the spatial distribution at 60-second intervals. For the low-α_0 case ($\alpha_0 = 0.5\ s^{-1}$, Fig. 4a), the effect of the

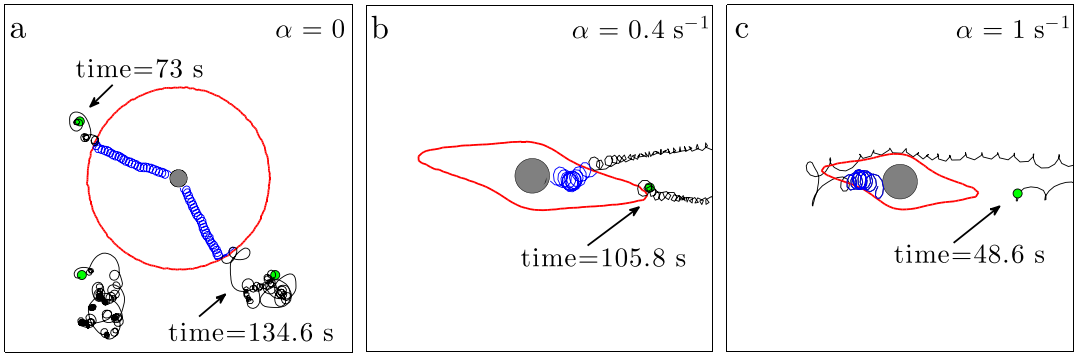

Fig. 10. Representative sperm paths for both the loitering (black) and response (blue) behaviors in 3 steady shear flows. The red line indicates the boundary for the threshold concentration. The times associated with a few sperm paths are indicated with the arrow. (For interpretation of the references to color in this figure legend, the reader is referred to the web version of this article.)

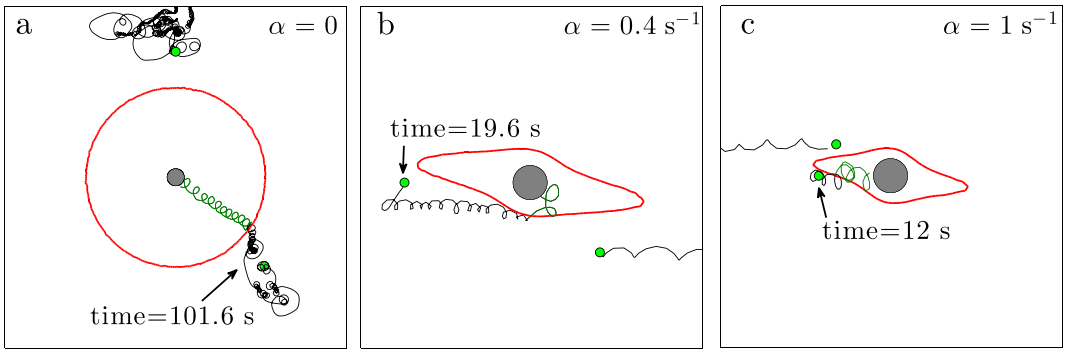

Fig. 11. Representative sperm paths for both the loitering (black) and response (green) behaviors in 3 steady shear flows. The red line indicates the boundary for the threshold concentration. The times associated with a few sperm paths are indicated with the arrow. (For interpretation of the references to color in this figure legend, the reader is referred to the web version of this article.)

unsteady shear is predominately to bend the protruding arms of the stretched chemoattractant plume. For this case, diffusion largely destroys any additional complexity at the ends of the arms (the Pe for this case, using $\alpha_0/2$ as an rms shear rate, is less than 4, and thus the effect of diffusion is relatively strong). For the high-α_0 case ($\alpha_0 = 1.25\ s^{-1}$, Fig. 4b), the Pe increases to approximately 10, and stirring by the unsteady shear produces significantly more complexity in the chemoattractant plume. Filaments are stretched and folded, with pronounced striations developing in the scalar field.

The chemoattractant plume distributions shown in Figs. 3 and 4 illustrate the range of concentrations (in units of mol L^{-1}) present around the egg. However, some of the concentrations are below the minimum threshold concentration required to elicit a behavioral response by sperm, and are functionally unimportant. Figs. 5 and 7 display the spatial extent of the portions of the plumes that would elicit sperm response for given values of the threshold. In the steady shear flow cases, Fig. 5 shows that for any shear rate, the effective plume area decreases as minimum threshold increases. The contour spacing also indicates information about the concentration gradients which will be useful when we look at the response behaviors in Section 3.2. Additionally, as the shear rate α increases, the effective plume area for any given threshold decreases. The effective egg target size caused by the diffusion and dispersion of the chemoattractant plume provides an evolutionary advantage (Jantzen et al., 2001; Levitan, 1993, 2000, 2006). We calculate an effective egg target diameter based on the area within a threshold concentration contour (A_s), and normalize this by the egg diameter as

$$D^* = \sqrt{4A_s/\pi} \Big/ \left(2R_{egg}\right). \tag{12}$$

The effect of steady shear rate on the normalized effective diameter is shown in Fig. 6 for three concentration thresholds. Both shear rate and threshold value decrease the size of the effective diameter as was seen qualitatively in Fig. 5.

In the unsteady shear flow cases, Fig. 7 shows a similar trend in the decrease in target area for increasing threshold concentration and shear rate. A new phenomenon occurs with the development of non-contiguous islands of above-threshold concentrations for Fig. 7b (high-α_0). It is likely that these would complicate or present challenges to search strategies for sperm seeking eggs. We calculate D^* for a few points in time in the high-α_0 unsteady shear flow and compare the values to D_c^*, the effective diameter calculated using Eq. (12) but now considering only the single contiguous area of the plume that contains the egg (Fig. 8). The values of D_c^* are typically smaller than D^*, but they remain large compared to unity, indicating that the plume effectively increases the target size from the perspective of the sperm. Nonetheless, it is clear that these islands of chemoattractant could pose an issue for sperm using the information for navigation. The impact of this area is further discussed in Section 3.2.

3.2. Sperm motility

In the absence of a chemoattractant stimulus, sperm exhibit a loitering behavior consisting of unbiased drifting circles. We begin by quantifying the relative dispersion of sperm due to this loitering behavior. Note that, due to their relatively large size, true diffusion of non-motile sperm in a molecular Brownian-motion sense is negligible. However, a collection of loitering sperm will disperse in space due to random differences in swimming directions. This dispersion has long been assumed to be diffusive (meaning that spatial variance grows linearly with time) in models of sperm motility (e.g., Keller and Segel, 1971). More recently, Inamdar et al. (2007) used dead and live sperm to demonstrate experimentally that sperm motility results in diffusive-

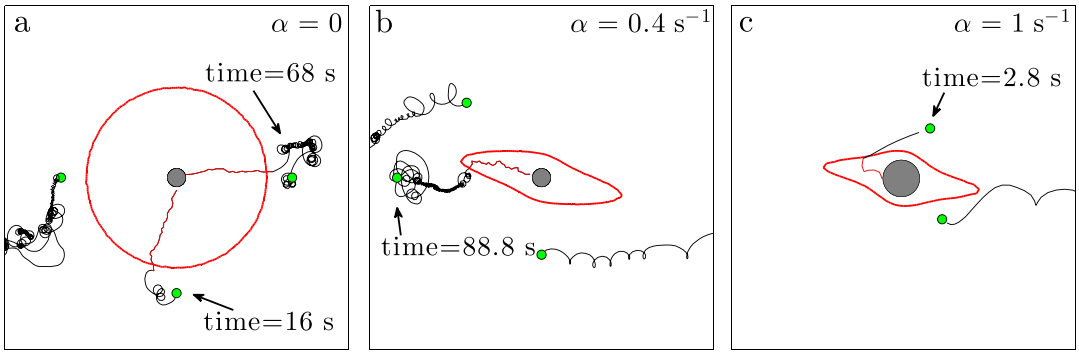

Fig. 12. Representative sperm paths for both the loitering (black) and response (red) behaviors in 3 steady shear flows. The red line indicates the boundary for the threshold concentration. The times associated with a few sperm paths are indicated with the arrow. (For interpretation of the references to color in this figure legend, the reader is referred to the web version of this article.)

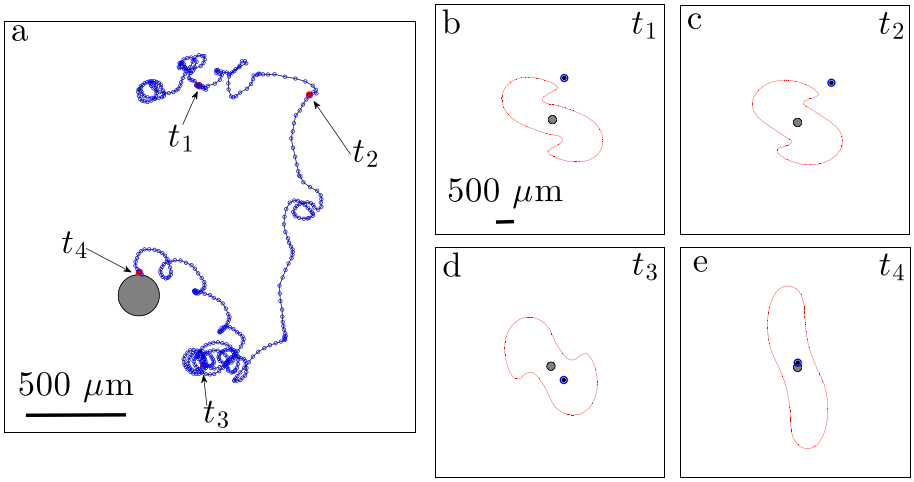

Fig. 13. Representative sperm path in the low-α_0 unsteady shear flow. The threshold contour boundary is indicated by a red line, the egg is represented by the centered gray circle and snapshots of the sperm location are shown by the blue circles. The scale in panel a is different. (For interpretation of the references to color in this figure legend, the reader is referred to the web version of this article.)

like spreading. A collection of sperm diffusing in two dimensions from a single point would have concentrations predicted by the solution to the 2D diffusion equation (Fischer et al., 1979)

$$C(x, y = 0) = \frac{M}{4\pi D_s t} \exp\left[-\frac{x^2}{4D_s t}\right], \tag{13}$$

where D_s is the effective diffusivity produced by motility. The resulting variance $\sigma^2 = 4D_s t$ would then grow linearly in time.

To investigate the dispersive behavior of sperm in our numerical model, we placed a large collection of loitering sperm at a single location in a quiescent flow and tracked their locations over time. Representative paths of three sperm over 30 s are shown in Fig. 9a. The variance growth of the entire sperm cloud is plotted in Fig. 9b as $\sigma^2/4$ vs. t. The linear trend indicates that the spreading is diffusive, with an effective diffusivity (given by the slope) of 1.8×10^{-9} m^2 s^{-1}. This is within the measured range of effective diffusivities obtained experimentally for urchin sperm by Inamdar et al. (2007).

Representative response behaviors in quiescent and steady shear flows are shown in Figs. 10–12 for each behavior. We quantify how quickly and how likely sperm are to reach the egg later in Section 3.3. The paths shown are real paths from the model, but they were specifically selected to show certain mechanisms (e.g., the flow sweeping the sperm passed the egg). Note that if a loitering sperm locates the threshold area, there is a very high chance of reaching the egg. In each case, the threshold concentration is indicated by the red lines and the 200 μm egg is indicated by the gray circle. The loitering part of the paths are shown in black, while the portion of the paths where the local concentration is above the threshold are highlighted by a specific color for each response.

Figs. 10a, 11a and 12a show a path for which the loitering sperm never locates the threshold contour, so therefore never initiates the response behavior. Additionally, paths associated with a successful sperm are shown with varying times indicated. For example, Fig. 10a shows two successful paths: one with a short path (total time to egg 73 s) and one with a longer path (134.6 s) to illustrate the range of times for sperm to locate an egg within the quiescent flow. In each of the steady shear flow cases (Figs. 10b, c, 11b, c, 12b and c) the path of a loitering sperm that is swept beyond the egg due to the flow is shown. Figs. 10b, c, 11b and 12c include the paths of sperm for which the flow instead brought the sperm towards the egg and aided in fertilization.

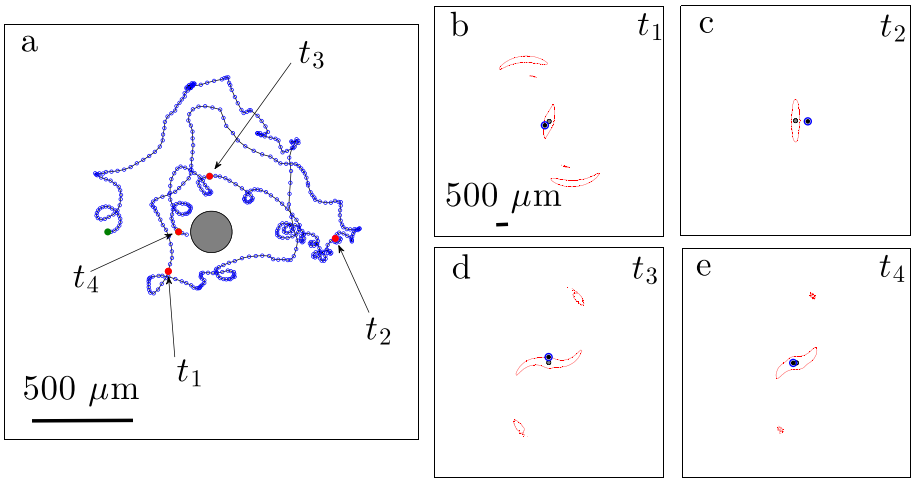

Fig. 14. Representative sperm path in the high-α_0 unsteady shear flow. The threshold contour boundary is indicated by a red line, the egg is represented by the centered gray circle and snapshots of the sperm location are shown by the blue circles. The scale in panel a is different. (For interpretation of the references to color in this figure legend, the reader is referred to the web version of this article.)

Sperm paths in the unsteady shear flows from the model are shown in Figs. 13–15. Each figure shows the entire path (a) with 4 instantaneous points in time highlighted in the subsequent plots (b–e). In each case, the blue circles indicates the sperm position every 0.1 s, the threshold concentration is indicated by the red lines and the 200 μm egg is indicated by the gray circle.

Fig. 13 illustrates a common case within the low-α_0 unsteady shear case wherein once the sperm locates the threshold concentration, it will remain within the higher concentration and likely locate the egg. The sperm loiters and advects with the flow in Fig. 13b, then locates the threshold area in Fig. 13c and remains within the higher concentration (Fig. 13d) before locating the egg (Fig. 13e). In the high-α_0 unsteady shear, the flow and fluctuating gradients may prevent sperm from staying within a filament of high concentration once it is located (Fig. 14c), but ultimately the egg can still be located (Fig. 14d and e). Additionally, Fig. 15 demonstrates the possible effect of the islands of threshold concentrations shown previously in Fig. 7. The sperm loiters (Fig. 15b) until it locates the chemoattractant (Fig. 15c) and then follows the gradients within this plume of isolated higher concentration (Fig. 15d and e), but that does not direct the sperm to the single egg. We quantify the impact for these isolated areas on the effective egg diameter in Fig. 8.

3.3. Fertilization rates

3.3.1. Steady shear

We present cumulative fertilization rate plots from a few cases that are representative of the overall results. In the quiescent flow, if a sperm locates the area of chemoattractant above the threshold, the subsequent likelihood of locating the egg is near 100%, though the timing depends on the strategy. The effect of the initial location on the fertilization rates is axisymmetric and is a function of the initial distance from the egg relative to the threshold radius for the quiescent flow. Fig. 16 shows all of the discussed initial locations for all results using one steady shear flow case as an example.

Fig. 17 shows the fertilization rates over 300 s for sperm using the Turn and Run Response. Representative paths of sperm swimming in the same flow using this response are shown above in Fig. 11 and the sperm all initiated from the same distance with the radial direction indicated by the Roman numeral in the top right of each plot, corresponding to the locations in Fig. 16. In the steady shear cases where $\alpha > 0$, shear rate enhances success at early times, but impedes success at late times, as seen in Fig. 17a where the higher shear rates have success in the first 75 s, but as time continues, the lower shear rates

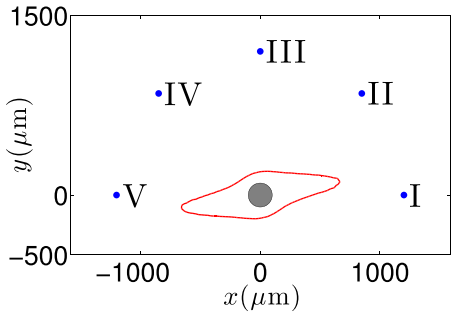

Fig. 16. All initial locations used to calculate the results are shown in Fig. 17. Note that the flow is axisymmetric and therefore positions I and V are in identical flow conditions. The radial distance from the center of the egg is $12R_{egg}$. The image shows the $\alpha = 0.4\ s^{-1}$ steady shear flow.

are eventually associated with higher success rates. The results are a representative case showing that the local flow velocity and direction can act to bring sperm close to the egg (Fig. 17a), sweep them past the egg (Fig. 17b and c), or allow the cloud of sperm to diffuse and overlap with the threshold concentration, allowing some sperm to locate the egg before being taken away from the egg (Fig. 17d and all quiescent cases).

Fig. 18 illustrates the fertilization rates for each response behavior in each steady shear case over 200 s. The sperm all started from the same point (I/V in Fig. 16). Corresponding representative paths of sperm swimming are shown above in Figs. 10–12. Again, it is seen that as shear increases, the success rates decrease. The target area of the chemoattractant decreases with increasing shear (as shown in Figs. 5 and 6), contributing to the decrease in fertilization success for higher shear rates. At later times, it should be noted that success rates decline because the sperm are swept passed the egg and then have little chance of returning since we have only considered one egg. This would not be the case for multiple eggs. In all flow cases, sperm utilizing any behavioral response are more likely to locate an egg than sperm with no response and the hierarchical order of behaviors is maintained (1. Run; 2. Turn and Run; 3. Drifting Circle) as seen in Fig. 18.

3.3.2. Unsteady shear

Fig. 19 provides a generalization of the fertilization rates within the unsteady flow using a few conditions. The rates are generally much lower in the high-α_0 unsteady shear case (Fig. 19b and c) compared to all of the steady shear flows (Fig. 18) and to the low-α_0 unsteady

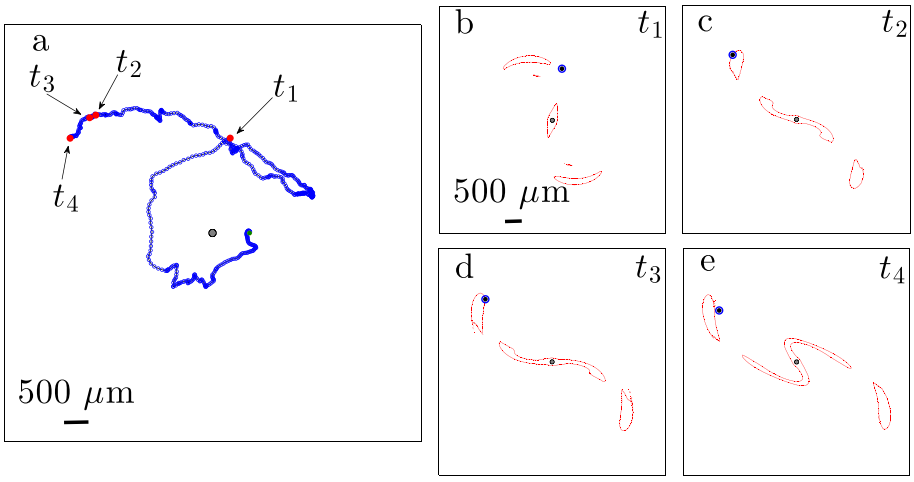

Fig. 15. Representative sperm path for a sperm in the high-α_0 unsteady shear case. The threshold contour boundary is indicated by a red line, the egg is represented by the centered gray circle and snapshots of the sperm location are shown by the blue circles. The scale in panel a is different. (For interpretation of the references to color in this figure legend, the reader is referred to the web version of this article.)

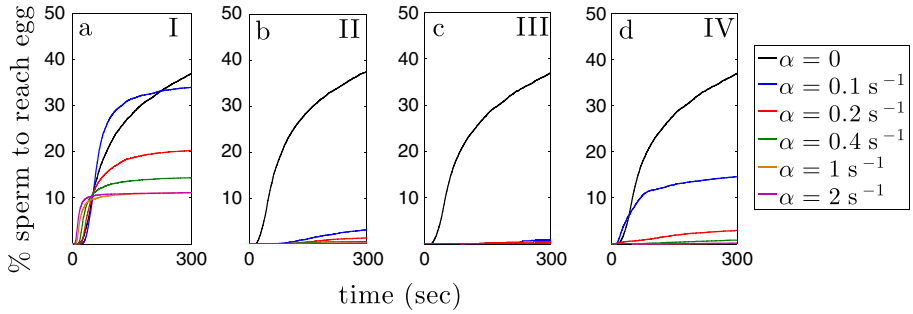

Fig. 17. Cumulative fertilization rates quantified for the Turn and Run Response over 300 s. The sperm began at the same point indicated by the roman numerals in the top right of each plot which correspond to the numerals in Fig. 16. Representative paths of sperm swimming in steady shear flows with the same response are shown above in Fig. 11.

shear cases (Fig. 19a). The higher shear rates, noted to reduce fertilization rates for the steady shear case, combined with the constantly evolving chemoattractant plume, where not all areas above the threshold lead to the egg and the gradient is not a simple path, decrease the ability of the sperm to reach the egg. However, the high-α_0 unsteady shear case does outperform the success rates in higher steady shear flows where the starting location is not ideal (compare to Fig. 18b and c). The sperm are less likely to be swept away within the unsteady shear because the strength and magnitude are not persistent as they are for the steady shear. In both unsteady shear flows, the Drifting Circle Response proved to be the least effective behavior, sometimes barely outperforming the no response case. This indicates that chemokinesis may be imperative to fertilization success in an unsteady flow.

4. Discussion

This study establishes a conceptual framework for a numerical model that incorporates flow around an egg, dispersion of chemoattractant from the egg and behavioral response of sperm navigating through the plume to find the egg. Sperm paths are produced from a phenomenological model to contribute to future holistic modeling approaches. There are clear idealizations in the model, many of which are associated with limitations in knowledge of the sensory and behavioral ecology of the sperm. Nonetheless, the results provide important insights and a foundation for understanding this fundamental physical–biological process.

The effect of shear and threshold concentration level on the effective target size of an egg are quantified and it is determined that an increase in either shear or concentration threshold level will reduce the perceived size of the egg. Insight is gained as to how chemoattractant plumes are perceived by sperm in unsteady shear and how complexity in the plume structure impacts the ability of sperm to locate eggs.

The results in the model indicate that any chemotactic and chemokinetic response provides an advantage over no response in almost every tested condition. A general hierarchy in the strategies used was constant over a range of conditions. The Run Response was the most successful behavior in any flow condition, but it is also the biggest change from the loitering behavior. The Turn and Run Response, while usually less likely to locate an egg, had generally similar fertilization rates and is perhaps a more natural strategy. The Drifting Circle Response is consistently less successful and does not perform well in flows with higher shear rates, suggesting that chemokinesis is indeed necessary for successful fertilization. With all factors considered, proximity to the egg and location within the flow are still the most significant element, highlighting the importance of stirring and mixing at a large scale as well as the diffusivity of a mass of sperm.

This study did not take into account the observed modulatory effect of shear on the ability of sperm to swim. A future study could include the effect of this behavior on cumulative fertilization rates. The ability of the sperm to reach only a single egg with a single chemoattractant plume was modeled. Multiple eggs with interacting and connected plumes would have a significant impact on the results as well.

Acknowledgment

This work was supported by the National Science Foundation (NSF) under Grant nos. 0849695 and 1205816.

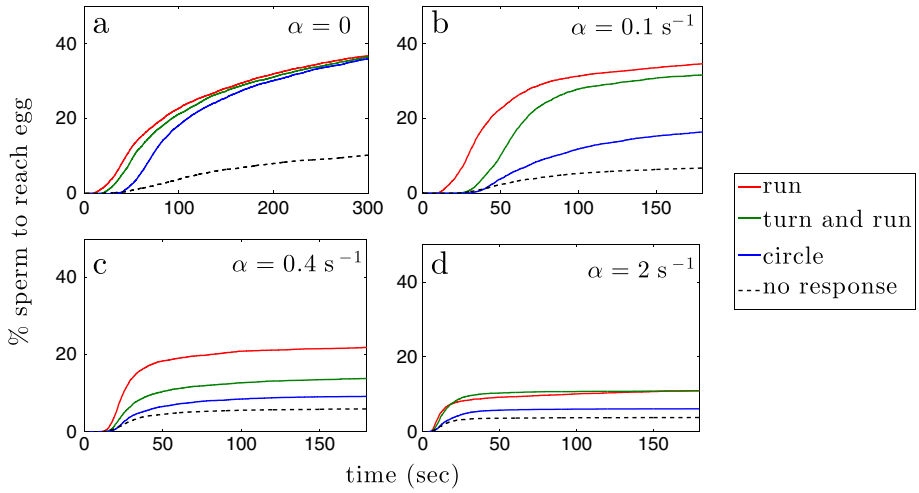

Fig. 18. Cumulative fertilization rates for each response behavior within each shear flow case quantified for 200 s. The sperm began at the same point (I/V in Fig. 16). Representative paths of sperm swimming in steady shear flows with the same response are shown above in Figs. 10–12.

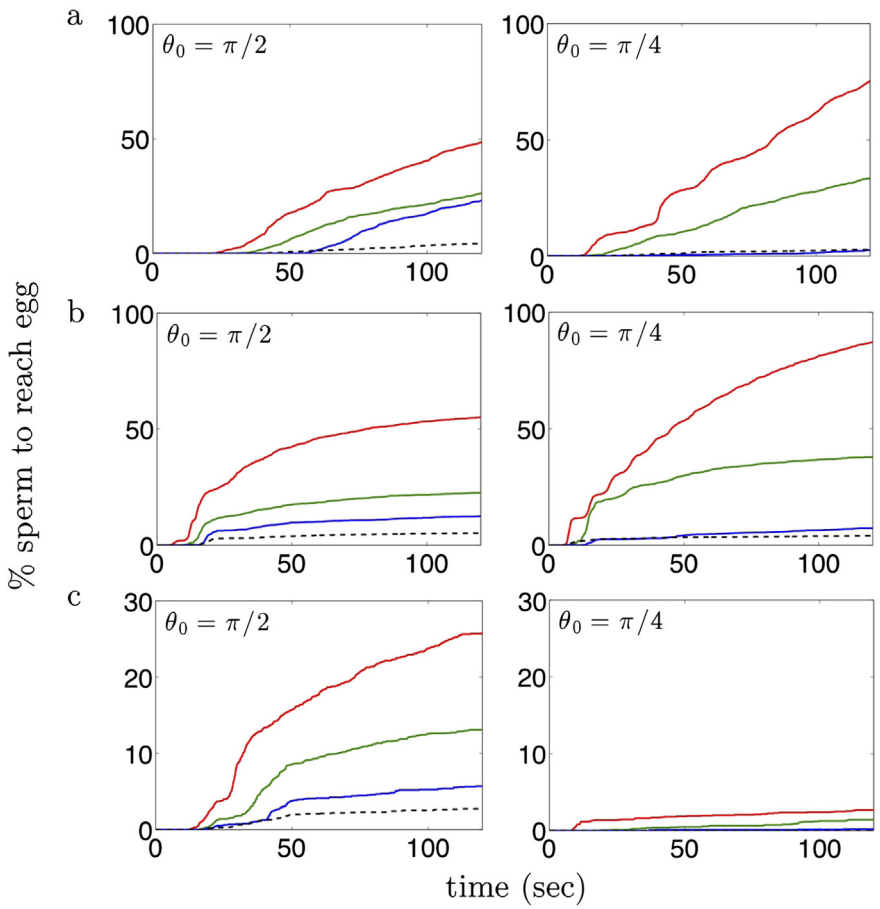

Fig. 19. Representative cumulative fertilization rates for the unsteady shear cases. Initial locations are indicated by the θ_0 term (the polar angle from the center of the egg) in the upper left corner of each plot: (a) Fertilization rates for the low-α flow case with initial radial distance $12R_{egg}$ from the center of the egg. (The rates all approach 100% in the low-α flow case when the sperm starts closer to the egg.) (b) High-α flow case with initial radial distance $6R_{egg}$ from the center of the egg. (c) High-α flow case with initial radial distance $12R_{egg}$ from the center of the egg. Note that the percentage scale in c ranges from 0–30%. Each behavioral response is shown (red line—Run; green line—Turn & Run; blue line—Drifting Circle; black dotted line—no response). (For interpretation of the references to color in this figure legend, the reader is referred to the web version of this article.)

Appendix A. Parameters

Table A.1
Parameter values used in models throughout the study.

Parameter	Value
Plume parameters	
$\sigma_{\dot{\phi}}$	$\pi/10\ s^{-1}$
T	60 s
R_{egg}	100 μm
r_{core}	$15R_{egg}$
D	$660\ \mu m^2\ s^{-1}$
Motile sperm parameters	
v_c	$150\ \mu m\ s^{-1}$
v_d	$20\ \mu m\ s^{-1}$
$\mu_{\dot{\theta}}$	$\pi\ s^{-1}$
Δ_{v_d}	$0.7\ \mu m\ s^{-1}$
Δ_{θ_d}	$3/\pi$
$\Delta_{\dot{\theta}}$	$1/\pi$
Δ_{θ_t}	$3/\pi$
Ψ^*	$2 \times 10^{-12}\ M\ \mu m^{-1}$

References

Alt, W., 1980. Biased random walk models for chemotaxis and related diffusion approximations. J. Math. Biol. 9, 147–177.

Alvarez, L., Dai, L., Friedrich, B.M., Kashikar, N.D., Gregor, I., Pascal, R., Kaupp, U.B., 2012. The rate of change in Ca^{2+} concentration controls sperm chemotaxis. J. Cell Biol. 196 (5), 653–663 (February).

Alvarez, L., Friedrich, B.M., Gompper, G., Kaupp, U.B., 2014. The computational sperm cell. Trends Cell Biol. 24 (3), 198–207 (March).

Babcock, R.C., Mundy, C.N., Whitehead, D., 1994. Sperm diffusion models and in situ confirmation of long-distance fertilization in the free-spawning asteroid *Acanthaster planci*. Biol. Bull. 186, 17–28 (February).

Basu, S., Barber, T., Cetegen, B., 2007. Computational study of scalar mixing in the field of gaseous laminar line vortex. Phys. Fluids 19 (5).

Benichou, O., Loverdo, C., Moreau, M., Voituriez, R., 2007. A minimal model of intermittent search in dimension two. J. Phys. Condens. Matter 19, 1–17 (January).

Benichou, O., Loverdo, C., Moreau, M., Voituriez, R., 2011. Intermittent search strategies. Rev. Mod. Phys. 83 (1), 81–129 (March).

Böhmer, M., Van, Q., Weyand, I., Hagen, V., Beyermann, M., Matsumoto, M., Hoshi, M., Hildebrand, E., Kaupp, U.B., 2005. Ca^{2+} spikes in the flagellum control chemotactic behavior of sperm. Eur. Mol. Biol. Organ. J. 24 (15), 2741–2752 (Aug).

Cetegen, B.M., Mohamad, N., 1993. Experiments on liquid-mixing and reaction in a vortex. J. Fluid Mech. 249, 391–414.

Cosson, M.P., Carre, D., Cosson, J., 1984. Sperm chemotaxis in siphonophores: calcium-dependent asymmetrical movement of spermatozoa induced by the attractant. J. Cell Sci. 68, 163–181.

Crimaldi, J.P., Zimmer, R.K., 2014. The physics of broadcast spawning in benthic invertebrates. Annu. Rev. Mar. Sci. 6 (1).

Crimaldi, J.P., Hartford, J.R., Weiss, J.B., 2006. Reaction enhancement of point sources due to vortex stirring. Phys. Rev. E 74 (July).

Crimaldi, J.P., Cadwell, J.R., Weiss, J.B., 2008. Reaction enhancement of isolated scalars by vortex stirring. Phys. Fluids 20 (July).

Denny, M.W., Shibata, M.F., 1989. Consequences of surf-zone turbulence for settlement and external fertilization. Am. Soc. Nat. 134 (6), 859–889 (December).

Denny, M., Dairki, J., Distefano, S., 1992. Biological consequences of topography on wave-swept rocky shores: I. enhancement of external fertilization. Biol. Bull. 183, 220–232 (October).

Denny, M.W., Nelson, E.K., Mead, K.S., 2002. Revised estimates of the effects of turbulence on fertilization in the purple sea urchin, *Strongylocentrotus purpuratus*. Biol. Bull. 203, 275–277 (December).

Evans, J.P., Garcia-Gonzalez, F., Almbro, M., Robinson, O., Fitzpatrick, J.L., 2012. Assessing the potential for egg chemoattractants to mediate sexual selection in a broadcast spawning marine invertebrate. Proc. R. Soc. B 279, 2855–2861 (March).

Farley, G.S., 2002. Helical nature of sperm swimming affects the fit of fertilization-kinetics model to empirical data. Biol. Bull. 203, 51–57 (August).
Farley, G.S., Levitan, D.R., 2001. The role of jelly coat in sperm-egg encounters, fertilization success and selection on egg size in broadcast spawners. Am. Soc. Nat. 157 (6), 626–636 (June).
Fischer, H., List, E., Koh, R., Imberger, J., Brooks, N., 1979. Mixing in Inland and Coastal Waters. Academic Press Inc.
Flohr, P., Vassilicos, J., 1997. Accelerated scalar dissipation in a vortex. J. Fluid Mech. 348, 295–317.
Friedrich, B.M., 2008. Search along persistent random walks. Phys. Biol. 5, 1–6 (June).
Friedrich, B.M., Julicher, F., 2007. Chemotaxis of sperm cells. Proc. Natl. Acad. Sci. U. S. A. 104 (33), 13256–13261 (August).
Friedrich, B.M., Julicher, F., 2008. The stochastic dance of circling sperm cells: sperm chemotaxis in the plane. New J. Phys. 10 (December).
Friedrich, B.M., Julicher, F., 2009. Steering chiral swimmers along noisy helical paths. Am. Phys. Soc. 103 (August).
Giorgi, A.E., DeMartini, J.D., 1977. A study of the reproductive biology of the red abalone, *Haliotis rufescens* Swainson, near Mendocino, California. Calif. Fish Game 63 (3), 80–94 (October).
Guerrero, A., Nishigaki, T., Carneiro, J., Tatsu, Y., Wood, C.D., Darszon, A., 2010a. Tuning sperm chemotaxis by calcium burst timing. Dev. Biol. 344, 52–56 (May).
Guerrero, A., Wood, C.D., Nishigaki, T., Carneiro, J., Darszon, A., 2010b. Tuning sperm chemotaxis. Biochem. Soc. Trans. 38 (5), 1270–1274 (Oct).
Himes, J.E., Riffell, J.A., Zimmer, C.A., Zimmer, R.K., 2011. Sperm chemotaxis as revealed with live and synthetic eggs. Biol. Bull. 220, 1–5 (February).
Inamdar, M.V., Kim, T., Chung, Y.K., Was, A.M., Xiang, X., Wang, C.W., Takayama, C., Lastoskie, C.M., Thomas, F.I.M., Sastry, A.M., 2007. Assessment of sperm chemokinesis with exposure to jelly coats of sea urchin eggs and resact: a microfluidic experiment and numerical study. J. Exp. Biol. 210, 3805–3820 (July).
Jabbarzadeh, E., Abrams, C.F., 2005. Chemotaxis and random motility in unsteady chemoattractant fields: a computational study. J. Theor. Biol. 235, 221–232 (January).
Jantzen, T.M., de Nys, R., Havenhand, J.N., 2001. Fertilization success and the effects of sperm chemoattractants on effective egg size in marine invertebrates. Mar. Biol. 138, 1153–1161 (April).
Jumars, P.A., Trowbridge, J.H., Boss, E., Karp_Boss, L., 2009. Turbulence–plankton interactions: a new cartoon. Mar. Ecol. 30, 133–150 (February).
Karp-Boss, L., Boss, E., Jumars, P.A., 1996. Nutrient fluxes to planktonic osmotrophs in the presence of fluid motion. Oceanogr. Mar. Biol. 34, 71–107.
Kaupp, U.B., Solzin, J., Hildebran, E., Brown, J.E., Helbig, A., Hagen, V., Beyermann, M., Pampaloni, F., Weyland, I., 2003. The signal flow and motor response controlling chemotaxis of sea urchin sperm. Nat. Cell Biol. 5, 109–117 (February).
Kaupp, U.B., Hildebrand, E., Weyland, I., 2006. Sperm chemotaxis in marine invertebrates—molecules and mechanisms. J. Cell. Physiol. 208, 487–494.
Kaupp, U.B., Kashikar, N.D., Weyand, I., 2008. Mechanisms of sperm chemotaxis. Annu. Rev. Physiol. 70, 93–117.
Keller, E.F., Segel, L.A., 1971. Model for chemotaxis. J. Theor. Biol. 30, 225–234 (February).
Kinzelbach, W., 1988. The random walk method in pollutant transport simulation. Groundw. Flow. Qual. Model. 227–245.
Kiselev, A., Ryzhik, L., 2012. Biomixing by chemotaxis and enhancement of biological reactions. Commun. Partial Diff. Equ. 37 (2), 298–318.
Krug, P.J., Riffell, J.A., Zimmer, R.K., 2009. Endogenous signaling pathways and chemical communication between sperm and egg. J. Exp. Biol. 212 (Pt 8), 1092–1100 (Apr).
Kupriyanova, E., Havenhand, J.N., 2002. Variation in sperm swimming behaviour and its effect on fertilization success in the serpulid polychaete *Galeolaria caespitosa*. Invertebr. Reprod. Dev. 41 (1-3), 21–26 (January).
Levitan, D., 1993. The importance of sperm limitation to the evolution of egg size in marine invertebrates. Am. Nat. 141, 517–536.
Levitan, D.R., 1996. Predicting optimal and unique egg sizes in free-spawning marine invertebrates. Am. Nat. 148 (1), 174–188 (July).
Levitan, D.R., 2000. Optimal egg size in marine invertebrates: theory and phylogenetic analysis of the critical relationship between egg size and development time in echinoids. Am. Nat. 156 (2), 175–192 (August).
Levitan, D.R., 2006. The relationship between egg size and fertilization success in broadcast-spawning marine invertebrates. Integr. Comp. Biol. 46 (3), 298–311 (March).
Levitan, D.R., Irvine, S.D., 2001. Fertilization selection on egg and jelly-coat size in the sand dollar *Dendraster excentricus*. Evolution 55 (12), 2479–2483.
Levitan, D.R., Young, C.M., 1995. Reproductive success in large populations: empirical measures and theoretical predictions of fertilization in the sea biscuit *Clypeaster rosaceus*. J. Exp. Mar. Biol. Ecol. 190, 221–241 (February).
Levitan, D.R., Sewell, M.A., Chia, F.S., 1991. Kinetics of fertilization in the sea urchin *Strongylocentrotus franciscanus*: interaction of gamete dilution, age and contact time. Biol. Bull. 181, 371–378 (December).
Levitan, D.R., Sewell, M.A., Chia, F.S., 1992. How distribution and abundance influence fertilization success in the sea urchin *Strongylocentotus franciscanus*. Ecol. Soc. Am. 73 (1), 248–254 (February).
Mark, P., Nilsson, L., 2002. A molecular dynamics study of tryptophan in water. J. Phys. Chem. 106, 9440–9445.
Martinand, D., Vassilicos, J., 2007. Fast chemical reaction and multiple-scale concentration fields in singular vortices. Phys. Rev. E 75 (3).
Meunier, P., Villermaux, E., 2003. How vortices mix. J. Fluid Mech. 476, 213–222.
Mikulencak, D.R., Morris, J.F., 2004. Stationary shear flow around fixed and free bodies at finite Reynolds number. J. Fluid Mech. 520, 215–242 (August).
Miller, K.J., Mundy, C.N., 2005. In situ fertilisation success in the scleractinian coral *Goniastrea favulus*. Coral Reefs 24 (2), 313–317 (March).
Morita, M., Nishikawa, A., Nakajima, A., Iguchi, A., Sakai, K., Takemura, A., Okuno, M., 2006. Eggs regulate sperm flagellar motility initiation, chemotaxis and inhibition in the coral *Acropora digitifera*, *A. gemnifera* and *A. tenuis*. J. Exp. Biol. 209, 4574–4579 (August).
Morita, M., Kitamura, M., Nakajima, A., Sri Susilo, E., Takemura, A., Okuno, M., 2009. Regulation of sperm flagellar motility activation and chemotaxis caused by egg-derived substance(s) in sea cucumber. Cell Motil. Cytoskeleton 66 (4), 202–214 (Apr).
Panton, R.L., 1996. Incompressible Flow: Second Edition. Second ed. Wiley & Sons.
Polson, A., 1937. On the diffusion constants of the amino-acids. Biochem. J. 31 (10), 1903–1912 (October).
Quinn, N.P., Ackerman, J.D., 2011. The effect of near-bed turbulence on sperm dilution and fertilization success of broadcast-spawning bivalves. Limnol. Oceanogr. Fluids Environ. 1, 176–193 (October).
Rehm, R., Baum, H., Tang, H., Lozier, D., 1993. Finite-rate diffusion-controlled reaction in a vortex. Combust. Sci. Technol. 91 (1-3), 143–161.
Riffell, J.A., Zimmer, R.K., 2007. Sex and flow: the consequences of fluid shear for sperm-egg interactions. J. Exp. Biol. 210 (Pt 20), 3644–3660 (Oct).
Riffell, J.A., Krugg, P.J., Zimmer, R.K., 2002. Fertilization in the sea: the chemical identity of an abalone sperm attractant. J. Exp. Biol. 205, 1439–1450 (February).
Riffell, J.A., Krug, P.J., Zimmer, R.K., 2004. The ecological and evolutionary consequences of sperm chemoattraction. Proc. Natl. Acad. Sci. U. S. A. 101 (13), 4501–4506 (January).
Styan, C.A., 1998. Polyspermy, egg size, and the fertilization kinetics of free-spawning marine invertebrates. Am. Nat. 152 (2), 290–297 (August).
Taylor, G., 1953. Dispersion of soluble matter in solvent flowing slowly through a tube. R. Soc. Lond. Proc. Ser. A 219, 186–203.
Vergassola, M., Villermaux, E., Shraiman, B.I., 2007. 'Infotaxis' as a strategy for searching without gradients. Nature 406–409 (January).
Vogel, H., Czihak, G., Chang, P., Wolf, W., 1982. Fertilization kinetics of sea urchin eggs. Math. Biosci. 58, 189–216.
Ward, G.E., Brokaw, C.J., Garbers, D.L., Vacquier, V.D., 1985. Chemotaxis of *Arbacia punctulata* spermatozoa to resact, a peptide from the egg jelly layer. J. Cell Biol. 101, 2324–2329 (December).
Wood, C.D., Nishigaki, T., Furuta, T., Baba, S.A., Darszon, A., 2005. Real-time analysis of the role of Ca^{2+} in flagellar movement and motility in single sea urchin sperm. J. Cell Biol. 169 (5), 725–731 (June).
Yoshida, M., Yoshida, K., 2011. Sperm chemotaxis and regulation of flagellar movement by Ca^{2+}. Mol. Hum. Reprod. 17 (8), 457–465 (Aug).
Yoshida, M., Inaba, K., Morisawa, M., 1993. Sperm chemotaxis during the process of fertilization in the ascidians *Ciona savignyi* and *Ciona intestinalis*. Dev. Biol. 157, 497–506 (January).
Yoshida, M., Murata, M., Inaba, K., Morisawa, M., 2002. A chemoattractant for ascidian spermatozoa is a sulfated steroid. Proc. Natl. Acad. Sci. U. S. A. 99 (23), 14831–14836.
Zimmer, R.K., Riffell, J.A., 2011. Sperm chemotaxis, fluid shear, and the evolution of sexual reproduction. Proc. Natl. Acad. Sci. U. S. A. 108 (32), 13200–13205 (Aug).